Bias-stress stability and radiation response of solution-processed AlO_x dielectrics investigated by on-site measurements

Y. X. Fang[1,2], C. Zhao[1,2,*], I. Z. Mitrovic[2], S. Hall[2], L. Yang[3,4], C. Z. Zhao[1,2,*]

[1]*Department of Electrical and Electronic Engineering, Xi'an Jiaotong-Liverpool University, Suzhou, China.*

[2]*Department of Electrical Engineering and Electronics, University of Liverpool, Liverpool, UK.*

[3]*Department of Chemistry, Xi'an Jiaotong-Liverpool University, Suzhou 215123, China.*

[4]*Department of Chemistry, University of Liverpool, Liverpool L69 7ZD, UK.*

**E-mail address of corresponding authors: Chun.Zhao@xjtlu.edu.cn; Cezhou.Zhao@xjtlu.edu.cn*

Abstract

In this work, the effects of biased irradiation on solution-processed and atomic layer deposited (ALD) AlO_x thin films MOS capacitors were investigated by an on-site technique. The devices were irradiated by a 662-KeV Cs^{137} γ-ray radiation source under different positive/negative gate biases. The radiation time was up to 10^5 s and the total dose was around 92 Gy. It has been found that radiation could result in reversibility of flat-band voltage shifts (ΔV_{FB}) of solution-processed AlO_x MOS capacitors, which were further analyzed through calculating the radiation induced oxide traps (ΔN_{ot}) in AlO_x thin film and interface traps at AlO_x/Si interface (ΔN_{it}). Additionally, solution-processed AlO_x MOS capacitors exhibit more radiation induced charges compared to those fabricated by ALD, which indicates that solution-processed AlO_x thin films contain abundant precursor impurities and bonded oxygen.

Keywords: Solution-processed; High-*k* gate dielectric; AlO_x; Biased γ-ray radiation stress stability.

1. Introduction

To date, solution processes have been developed due to the possibility of low-cost and large-area fabrication without using vacuum deposition techniques. Furthermore, solution-processed high-*k* oxide dielectrics enable low leakage current, low operation voltage and ease of process integration for associated thin-film transistors (TFTs) [1]. Among the various high-k materials, Al_2O_3 is a promising candidate, due to its good chemical stability and low oxide/semiconductor interface trap density in a TFT device [2]. High temperature (>300 ºC) annealed high-*k* oxide materials exhibit satisfactory film quality, electrical properties and reliability. However, their potential applications towards wearable electronics and bioelectronics are further restrained due to the high annealing temperature required in the fabrication [3]. As a result, it is necessary to investigate the bias-stress stability and radiation response of solution-processed high-*k* oxide materials annealed at low temperature (<150 ºC). In addition, low temperature processing with simplified process steps is the primary advantage of solution-process compared to traditional vacuum fabrication methods.

In general, for a TFT, ionizing radiation could lead to device degradation by generating bulk oxide and interface traps near the oxide/semiconductor interface [4]. There have been few reported studies addressing radiation damage to solution-processed high-*k* materials for TFT application [5]. It should be noted that the interruption of irradiation in conventional off-site radiation response measurements can cause a rapid recovery of flat band voltage (V_{FB}) shift so that the degradation caused by charge trapping/de-trapping of the devices is underestimated [6]. As a result, on-site measurements are required and to our knowledge, no research has been reported on the study of γ-ray radiation response of solution-processed high-*k* materials investigated by an on-site technique.

In this work, solution-processed and atomic layer deposited (ALD) AlO_x thin films were fabricated for comparison. They were integrated into capacitors to investigate bias-stress stability along with radiation response through the on-site technique [7].

2. Experimental

2.1 Precursor Preparation

The precursor solution was prepared by dissolving 2.5M concentration aluminum nitrate hydrate ($Al(NO_3)_3 \cdot xH_2O$) in water. The solution was stirred in ultrasonic bath for 2 h to ensure the precursor was fully dissolved since the nitrate salts show excellent water solubility. Before spin coating, the solution was filtered by a 0.45 μm polyether sulfone (PES) syringe filter.

2.2 Device fabrication

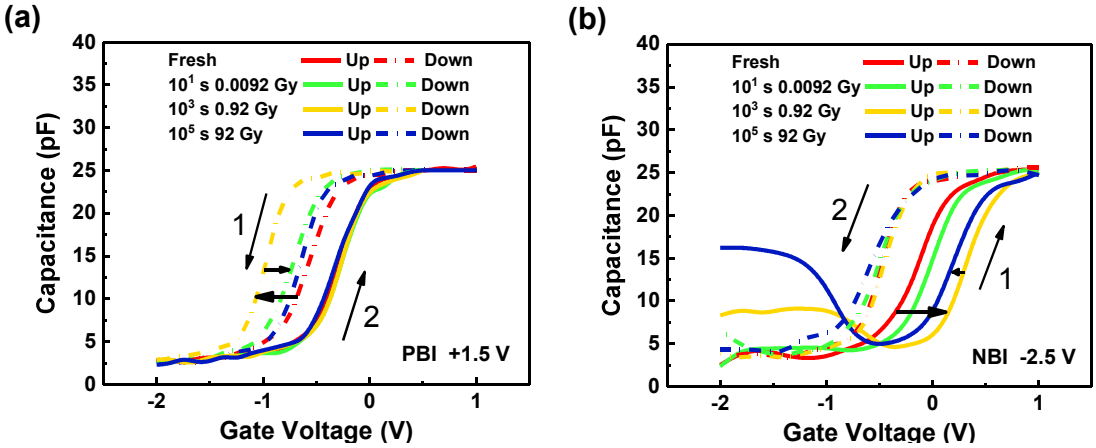

*Figure 1. Capacitance-voltage (C-V) curves of solution-processed AlO_x MOS capacitors (annealed at 100 °C) under 10^5 s gate bias-stress voltage of **(a)** +1.5 V positively biased irradiation (PBI) and **(b)** -2.5 V negatively biased irradiation (NBI). The total dose is around 92 Gy.*

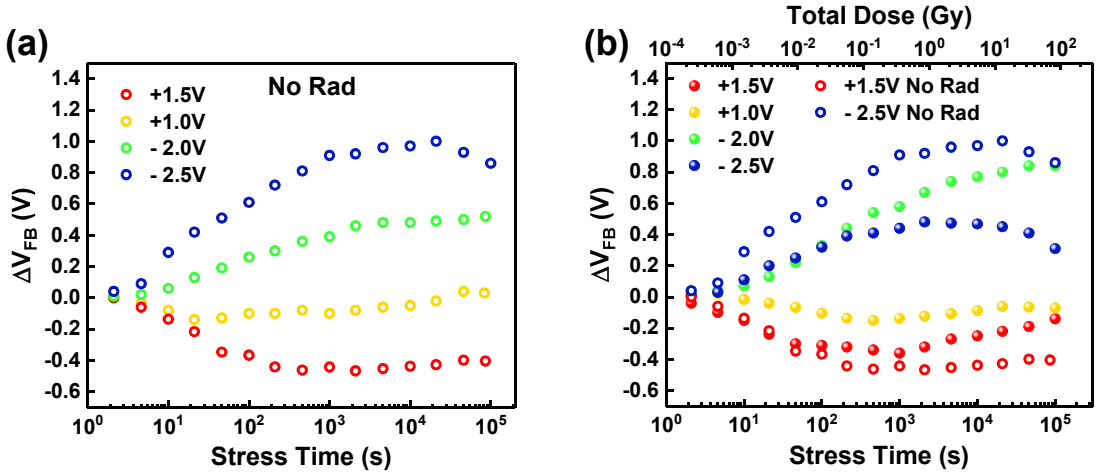

*Figure 2. Flat-band voltage shift (ΔV_{FB}) of solution-processed AlO_x capacitors induced by different positive/negative bias-stress as a function of **(a)** stress time, **(b)** stress time & total dose. ΔV_{FB} was extracted from C-V curves measured from AlO_x capacitors at 1MHz.*

Before spinning-coating, lightly-doped N type Si substrates (resistivity: 2-4 Ω·cm, impurity density: 1.65×10^{15} cm^{-3}) were dipped in 2% HF aqueous solution for 60 s to remove the native oxide, and dried by N_2. Subsequently, the substrates were exposed to air plasma for 15 mins. After preparation of Si substrates, the precursor solution was spin-coated on the processed substrate at 4500 rpm for 40 s. Samples were then immediately annealed on the hot plate at 100 °C for 1 h in air atmosphere. Finally, 300 nm thick Al top and bottom electrodes were deposited through shadow masks by e-beam evaporation. The circular top electrode had a diameter of 0.3 mm.

2.3 Characterization

The thickness of the AlO_x thin films was measured by spectroscopic ellipsometry. Solution-processed and ALD AlO_x thin films are 50 nm and 40 nm thick, respectively. The capacitance-voltage (C-V) characteristics were measured using a HP 4284 precision LCR meter at a frequency of 1 MHz. To investigate the bias-stress and biased irradiation stability of AlO_x MOS capacitor, constant voltage bias stress was applied on the gate with and without radiation exposure. The bias-stress voltage is the voltage applied on the gate during the bias-stress. C-V curves were measured at regular points in time of $10^{1/3}$ s, $10^{2/3}$ s, $10^{3/3}$ s, $10^{4/3}$ s, $10^{5/3}$ s etc. to allow extraction of the V_{FB} during the bias-stress. For biased irradiation, a 662-keV Cs^{137} γ-ray radiation source was used, the stress time was up to 10^5 s and the total dose was around 92 Gy. All electrical measurements were carried out in the dark at room temperature.

3. Results and Discussion

The C-V curves of solution-processed AlO_x MOS capacitors under 10^5 s gate bias-stress voltage of irradiated +1.5 V and irradiated -2.5 V are shown in Figs. 1 (a) and (b), respectively. It can be seen that the shift of the C-V curves, positive or negative, is determined by the gate bias stress polarity. Positively biased irradiation (PBI) and negatively biased irradiation (NBI)

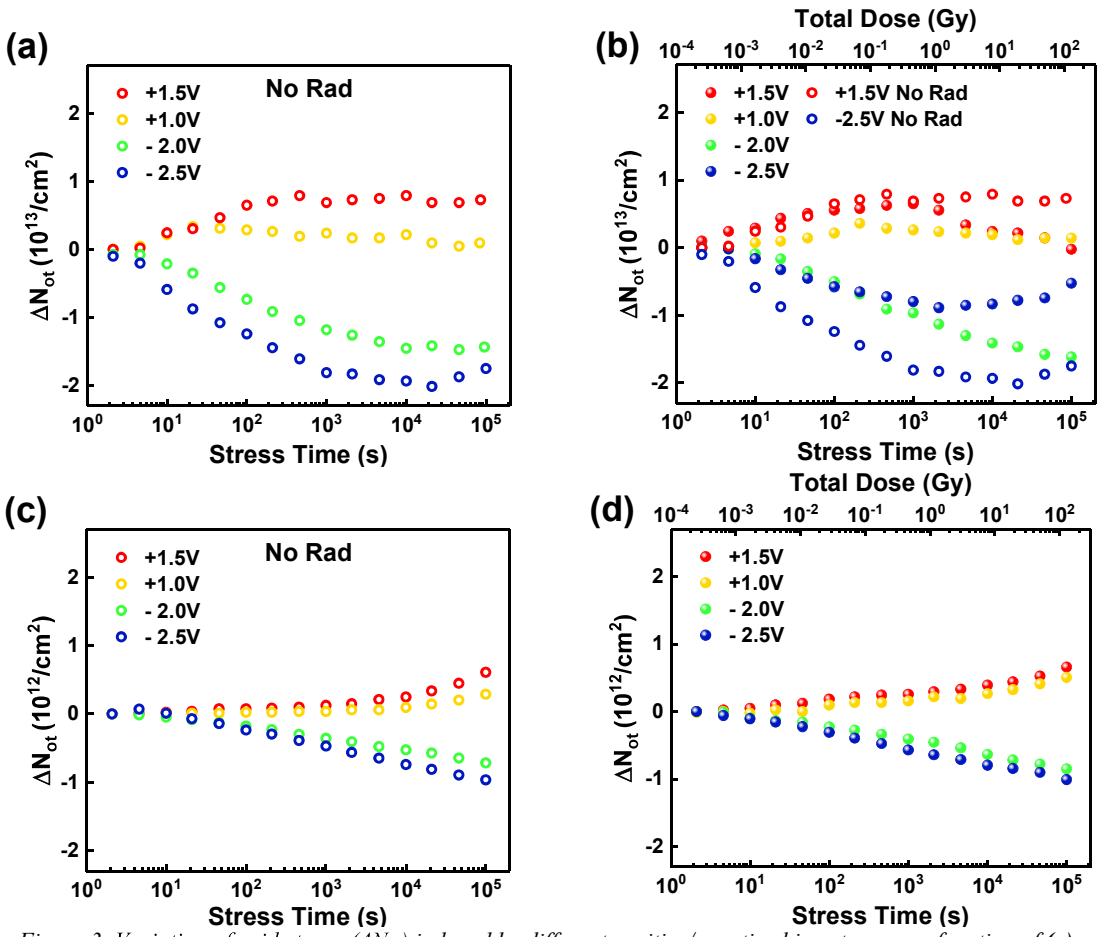

*Figure 3. Variation of oxide traps (ΔN_{ot}) induced by different positive/negative bias-stress as a function of **(a)** stress time (solution-processed AlO_x), **(b)** stress time & total dose (solution-processed AlO_x), **(c)** stress time (ALD AlO_x) and **(d)** stress time & total dose (ALD AlO_x).*

produce negative and positive flat-band voltage shift (ΔV_{FB}), respectively. To determine V_{FB}, flat band capacitance (C_{FB}) is calculated first, then left flat-band voltage ($V_{FB\ L}$) and right flat-band voltage ($V_{FB\ R}$) can be determined from the left and right C-V curves of the MOS devices, respectively. It is found in Fig. 1(a) that the degradation of C-V curves is mainly caused by $\Delta V_{FB\ L}$ under PBI. Under NBI, as shown in Fig. 1(b), $\Delta V_{FB\ R}$ dominates the device degradation. Consequently, $\Delta V_{FB\ L}$ under PBI and ΔV_{FBR} under NBI are further investigated by consideration of the hysteresis. In addition, ΔV_{FB} is found to increase first when the stress time is less than 10^3 and then decrease as the stress time increases from 10^3 s to 10^5 s. This reversible behavior indicates that the ΔV_{FB} is mainly caused by the bias-stress induced charges in short stress time (< 10^3 s). As the stress time increases (10^3 s ~ 10^5 s), the radiation generated charges becomes dominate and can compensate the bias-stress induced charges, thus cause ΔV_{FB} to decrease.

Plots of ΔV_{FB} under gate bias-stress with and without radiation are shown in Fig. 2. The radiation-induced ΔV_{FB} is determined by the generation of oxide traps (ΔN_{ot}) in the AlO_x film and interface traps (ΔN_{it}) at the AlO_x/Si interface. The ΔN_{ot} causes a parallel shift of both mid-gap and flat band voltages, ΔN_{it} determines the stretch-out of the C-V curve and only shifts the flat band voltage [8].

Figs. 3 (a) and (b) summarize the ΔN_{ot} of solution-processed AlO_x capacitors under gate bias with and without radiation. ΔN_{ot} is estimated as [9]:

$$\Delta N_{ot} = -\frac{C_{ox}\Delta V_{mg}}{qA} \qquad (1)$$

where C_{ox} is oxide capacitance, ΔV_{mg} is shift of mid gap voltage, q is elemental charge and A is the area of the device. Under PBI, positive ΔN_{ot} decreases with increasing radiation dose, indicating that the radiation has generated negative oxide trapped charges. Under NBI, a decrease of ΔN_{ot} can also be observed. Furthermore, with a larger gate bias, the decreasing of ΔN_{ot} becomes more obvious. These results suggest that bias-stress enhances the effect of radiation, which will be discussed later with the aid of the energy band diagrams in Fig. 5. The ΔN_{ot} of ALD AlO_x capacitors with and without radiation are shown in Figs. 3 (c) and (d). These

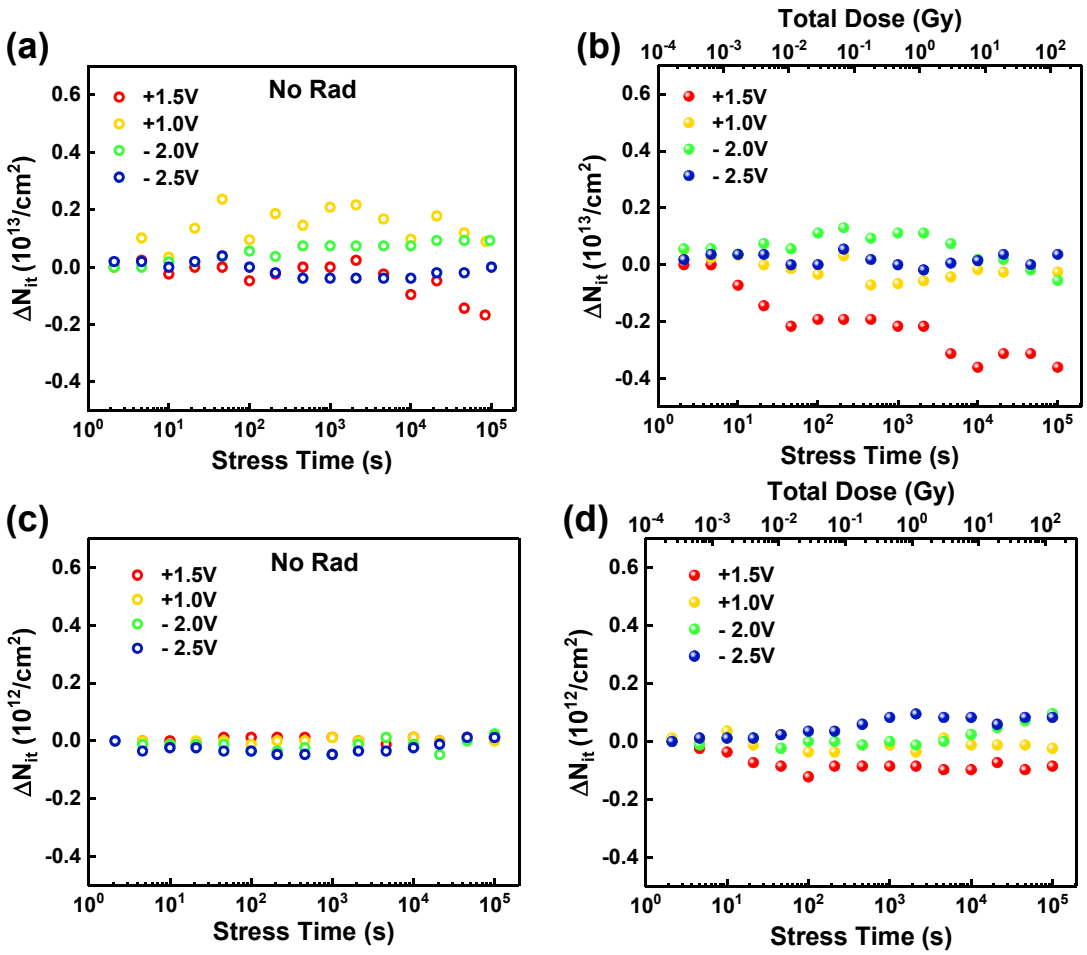

Figure 4. Variation of interface traps (ΔN_{it}) induced by different positive/negative bias-stress as a function of ***(a)*** *stress time (solution-processed AlO_x),* ***(b)*** *stress time & total dose (solution-processed AlO_x),* ***(c)*** *stress time (ALD AlO_x) and* ***(d)*** *stress time & total dose (ALD AlO_x).*

devices reveal small ΔN_{ot} and no significant changes or reversibility are observed, indicating better radiation hardness relative to solution-process AlO_x. It is reported that solution-processed, low temperature AlO_x contains a large concentration of bonded oxygen, which could provide defect states in the bandgap of AlO_x [2].

Figs. 4 (a) and (b) present the ΔN_{it} of solution-processed AlO_x capacitors under gate bias-stress with and without radiation. ΔN_{it} is estimated as [9]:

$$\Delta N_{it} = \frac{C_{ox}(\Delta V_{FB} - \Delta V_{mg})}{qA} \qquad (2)$$

Under PBI, the devices exhibit a build-up of Si dangling bonds, which is related to the protons released by radiation. Under NBI, there is a negligible change of ΔN_{it} because PB is necessary to generate interface traps under radiation exposure. The mechanism will be explained in the next section. Furthermore, ΔN_{it} of ALD AlO_x capacitors is shown in Figs. 4 (c) and (d). Similar to the associated ΔN_{ot} results, biased irradiation generates very few interface traps. This is likely to be due to the low defect state density in ALD AlO_x thin films.

As ALD AlO_x thin films have exhibited satisfied radiation hardness. The radiation mechanism of solution-processed AlO_x thin films is further investigated in this work. Figs. 2 have illustrated a reversible behavior of ΔV_{FB} of solution-processed devices. The reversibility of ΔV_{FB} is associated with the combined effect of ΔN_{ot} and ΔN_{it}.

Fig. 5 (a) and (b) demonstrates the energy band diagrams of solution-processed AlO_x MOS capacitors under (a) PBI and (b) NBI, respectively. Under PBI, when the PBI time is shorter than 10^3 s, electrical bias causes a negative ΔV_{FB} by generating positive ΔN_{ot} and radiation exposure can barely affect the device degradation. However, as shown in Fig. 5 (a), neutral oxide traps are created in the bulk of the AlO_x during exposure to ionizing irradiation [10]. With a positively applied gate voltage, electrons in the accumulation region at the AlO_x/Si interface can tunnel into those radiation induced neutral oxide traps (process (2) in Fig. 5(a)). The effects of bias-stress and irradiation add up and form negatively charged traps, which can compensate the positive oxide trapped charges near the AlO_x/Si interface, thus reduce positive ΔN_{ot} [11, 12]. Consequently,

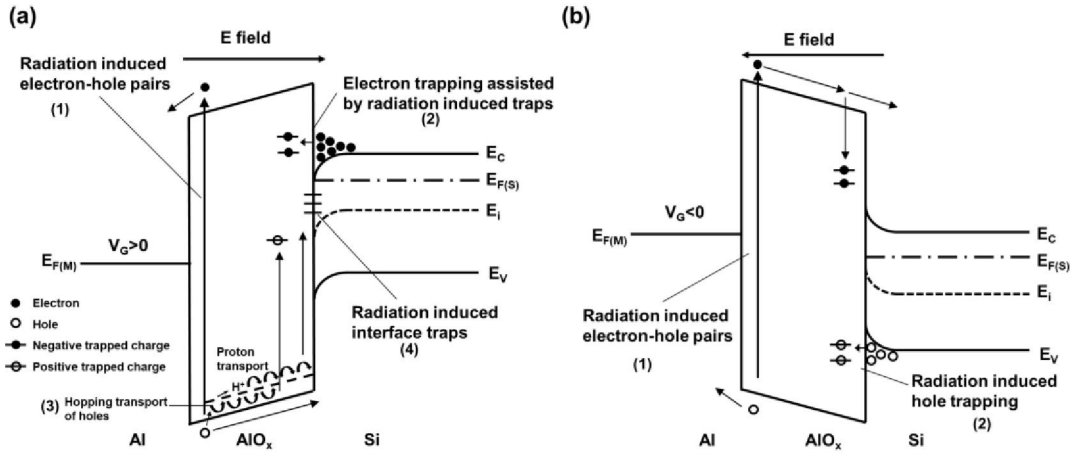

*Figure 5. Energy band diagrams of solution-processed AlO_x capacitors under **(a)** PBI and **(b)** NBI.*

when the PBI time increases from 10^3 s to 10^5 s, radiation induced electron trapping among the oxide dominates the device degradation and causes a positive ΔV_{FB} as well as a negative ΔN_{ot}.

Furthermore, when radiation passes through a gate oxide, electron/hole pairs are created (process (1) in Fig. 5 (a)) [13]. The radiation-induced electrons escape from the oxide within several picoseconds due to their higher mobility relative to holes. Radiation induced holes could transport towards the AlO_x/Si interface under PBI, and liberate hydrogen, in the form of protons [14] which reach the interface by hopping transport (process (3) in Fig. 5 (a)). The protons can react, break existing Si-H bonds to form H_2 and a trivalent Si defect thus causing ΔN_{it} to increase, as shown in Fig. 4 (b). As mentioned earlier, the PB is necessary for the de-passivation. Applying a NB will inhibit the proton from drifting to the interface and the de-passivation of Si-H bonds by H at the interface is suppressed [15]. This could be the reason why ΔN_{it} is found to build up under PBI, and stay approximately constant under NBI in Fig. 4 (b).

Under NBI, when the stress time is shorter than 2×10^3 s, some of the electrons injected from the gate electrode into the oxide under the applied electrical field. They fall into traps to form negative trapped charges and cause a positive ΔV_{FB}. Meanwhile, radiation exposure can barely affect the device degradation. However, as shown in Fig. 5 (b), in a similar manner to the PBI condition, accumulated holes at the AlO_x/Si interface could tunnel from Si to radiation-induced defects in the oxide to form positive oxide trapped charges (process (2) in Fig. 5 (b)), which results in a negative ΔV_{FB} and a positive ΔN_{ot} as the NBI time increases from 2×10^3 s to 10^5 s.

From the analysis above, radiation induces a large concentration of shallow oxide traps and causes the generation of interface traps by releasing protons in solution-processed AlO_x capacitors, thus shifting V_{FB} and degrading the solution-processed AlO_x MOS capacitors. On the other hand, ALD AlO_x capacitors show good radiation hardness and no reversibility of ΔV_{FB} is observed with biased irradiation. The possible reason is that the solution-process brings abundant precursor impurities during fabrication.

4. Conclusion

Solution-processed and atomic layer deposited AlO_x thin films were fabricated at low temperature. The effects of biased irradiation on AlO_x based MOS capacitors were investigated by an on-site technique. It has been found that radiation can result in reversibility of ΔV_{FB} of solution-processed AlO_x MOS capacitors, which is further analyzed by extracting the radiation induced oxide (ΔN_{ot}) and interface (ΔN_{it}) traps at AlO_x/Si interface. The results suggest that, compared to the ALD AlO_x films, solution-processed AlO_x thin films contain abundant precursor impurities.

Acknowledgments

This research was funded in part by the Key Program Special Fund in XJTLU (KSF-P-02, KSF-A-05, KSF-A-07 and KSF-T-03). The author IZM acknowledges UKRI GIAA award as well as British Council UKIERI project no. IND/CONT/G/17-18/18.

References

[1] W. Xu, M. Long, T. Zhang, L. Liang, H. Cao, D. Zhu, J.-B. Xu, Ceramics International 43 (2017) 6130-6137.
[2] A. Liu, G. Liu, H. Zhu, B. Shin, E. Fortunato, R. Martins, F. Shan, RSC Advances 5 (2015) 86606-86613.
[3] H.-R. Byun, E.-A. You, Y.-G. Ha, Appl Phys Lett 114 (2019) 013301.
[4] R. Lok, S. Kaya, H. Karacali, E. Yilmaz, Radiat Phys Chem 141 (2017) 155-159.

[5] B. Park, D. Ho, G. Kwon, D. Kim, S. Y. Seo, C. Kim, M.-G. Kim, Adv Funct Mater 28 (2018) 1802717.
[6] Y. Mu, C. Z. Zhao, Q. Lu, C. Zhao, Y. Qi, S. Lam, I. Z. Mitrovic, S. Taylor, P. R. Chalker, IEEE T Nucl Sci 64 (2017) 673-682.
[7] Y. Mu, C. Z. Zhao, Y. Qi, S. Lam, C. Zhao, Q. Lu, Y. Cai, I. Z. Mitrovic, S. Taylor, P. R. Chalker, Nucl Instrum Meth B 372 (2016) 14-28.
[8] A. Kahraman and E. Yilmaz, Radiat Phys Chem 139 (2017) 114-119.
[9] J. A. Felix, D. M. Fleetwood, R. D. Schrimpf, J. G. Hong, G. Lucovsky, J. R. Schwank, M. R. Shaneyfelt, IEEE T Nucl Sci 49 (2002) 3191-3196.
[10] M. Ceschia, A. Paccagnella, A. Cester, A. Scarpa, G. Ghidini, IEEE T Nucl Sci 45 (1998) 2375-2382.
[11] D. A. Neamen, IEEE T Nucl Sci 31 (1984) 1439-1443.
[12] T. Stanley, D. Neamen, P. Dressendorfer, J. Schwank, P. Winokur, M. Ackermann, K. Jungling, C. Hawkins, W. Grannemann, IEEE T Nucl Sci 32 (1985) 3982-3987.
[13] T. R. Oldham and F. B. McLean, IEEE T Nucl Sci 50 (2003) 483-499.
[14] X. J. Zhou, D. M. Fleetwood, L. Tsetseris, R. D. Schrimpf, S. T. Pantelides, IEEE T Nucl Sci 53 (2006) 3636-3643.
[15] D. Cao, X. Cheng, T. Jia, L. Zheng, D. Xu, Z. Wang, C. Xia, Y. Yu, D. Shen, IEEE T Nucl Sci 60 (2013) 1373-1378.